Available online at www.sciencedirect.com
SCIENCE DIRECT®
Journal of Organometallic Chemistry 681 (2003) 37–50
Journal of Organometallic Chemistry
www.elsevier.com/locate/jorganchem

Supported rhodium nanoparticles in catalysis: the role of stabilizers on catalytic activity and structural features

Giovanni Vitulli [a,*], Claudio Evangelisti [a], Paolo Pertici [a], Anna Maria Caporusso [a], Nicoletta Panziera [a], Piero Salvadori [a], Maria Giulia Faga [b], Chiara Manfredotti [b], Gianmario Martra [b], Salvatore Coluccia [b], Antonella Balerna [c], Stefano Colonna [d], Settimio Mobilio [c,e]

[a] *Istituto per la Chimica dei Composti OrganoMetallici, ICCOM-CNR, Sezione di Pisa, c/o Dipartimento di Chimica e Chimica Industriale dell'Università di Pisa, via Risorgimento 35, 56126 Pisa, Italy*
[b] *Dipartimento di Chimica I.F.M., Università di Torino, via P. Giuria 7, 10125 Torino, Italy*
[c] *INFN-Laboratori Nazionali di Frascati, Via E. Fermi 40, 00044 Frascati, Roma, Italy*
[d] *CNR-Istituto di Struttura della Materia, Via Fosso del Cavaliere 100, 00133 Roma, Italy*
[e] *Dipartimento di Fisica, Universita' di Roma Tre, Via della Vasca Navale 84, 00146 Roma, Italy*

Received 10 March 2003; received in revised form 8 May 2003; accepted 8 May 2003

Abstract

Rhodium nanoparticles supported on γ-Al_2O_3, derived from arene-solvated Rh atoms stabilized by trioctylamine (TOA), are valuable catalysts in hydrogenation and silylformylation reactions. They are largely more active than the analogous commercial catalyst, as well as of a sample similarly prepared in the absence of TOA. HRTEM measurements, IR studies on adsorbed CO species and extended X-ray absorption fine structure analyses evidenced the role of TOA in controlling the particle growth in the preparative process and in stabilizing the resulting Rh particles against erosion by CO and oxidation.
© 2003 Elsevier Science B.V. All rights reserved.

Keywords: Supported rhodium nanoparticles; Trioctylamine; Metal vapour synthesis; Catalysis; Surface properties

1. Introduction

Recently, there has been a great deal of attention on the use of metal nanoparticles as valuable catalysts [1]. Their catalytic properties are strongly related to the particle size and recent findings on their size-dependent chemistry has added a new dimension to the subject [2]. However, stabilizers are usually used to avoid agglomeration to bulk metal and the kind of stabilizer can also strongly affect their catalytic behaviour [3]. In the hydrogenation reaction, for instance, strong interacting ligands, like tetraalkylammonium halides, poly-*N*-vinyl-2-pyrrolidone, 1,10-phenantroline, have been found to restrict the catalytic activity [1j], while hydroxyalkyl ammonium salts or aliphatic amines with long alkyl groups (C_8 or higher) have been reported to greatly improve the efficiency of the catalytic precursor [1i,4]. Moreover, solvent-stabilized metal microclusters, obtained by reaction of metal vapour with weakly coordinating organic ligands (acetone, tetrahydrofuran, toluene, etc.) (solvated metal atoms), are very active homogeneous catalytic precursors in a wide range of reactions, including hydrogenation, hydrosilylation, hydroformylation, silylformylation and oligo-polymerization of olefins and acetylenes [1c,1l,5]. With the aim to provide a further insight into the subject, we have

* Corresponding author. Present address: Istituto per la Chimica dei Composti Organo Metallici, ICCOM-CNR, Sezione di Pisa, via Risorgimento 35, Pisa 56125, Italy. Tel.: +39-050-918224; fax: +39-050-918260.
E-mail address: pervit@server1.dcci.unipi.it (G. Vitulli).

0022-328X/03/$ - see front matter © 2003 Elsevier Science B.V. All rights reserved.
doi:10.1016/S0022-328X(03)00529-1

studied the activity of catalysts prepared from arene-solvated Rh atoms, containing trioctylamine (TOA) as additional stabilizer. Such systems are excellent starting materials for the preparation of new supported catalysts largely more active and selective than analogous samples commercially available or similarly prepared in the absence of TOA. We report here evidence for their peculiar catalytic properties and some data on their structural features. For this, the catalysts have been characterized by HRTEM analyses, IR studies on adsorbed CO species and extended X-ray absorption fine structure (EXAFS) investigations.

2. Experimental

2.1. General

All operations involving the metal vapour synthesis (MVS) products were performed under a dry argon atmosphere. The co-condensation of rhodium and mesitylene was carried out in a static reactor previously described [6]. The "mesitylene-solvated Rh atoms" solution was worked up under argon atmosphere with the use of the standard Schlenk techniques. The amount of rhodium in the above solutions was determined by atomic absorption spectrometry in a electrochemically heated graphite furnace with a Perkin–Elmer 4100ZL instrument. Solvents were purified by conventional methods, distilled and stored under argon. TOA, cinnamaldehyde, methyl benzoate, 1-hexyne were commercial products and were degassed and stored under argon before use. Commercial γ-Al_2O_3 (Chimet product, type 49, surface area 110 $m^2\ g^{-1}$, mean particle diameter 31 μm) was dried in a static oven before use. Commercial rhodium on γ-Al_2O_3 (5 wt.% of Rh, surface area 130 $m^2\ g^{-1}$) was an Engelhardt product.

The infrared spectra of adsorbed CO studies were obtained with a Bruker IFS-28 spectrometer with MCT detector (128 scans, resolution 4 cm^{-1}). H_2 and CO with high-purity grade were used without further purification. The samples, in the form of self-supporting pellet, were put into an IR quartz cell with KBr windows and outgassed at room temperature (r.t.) for 50 min (residual pressure into the vacuum line $< 10^{-5}$ Torr). After that, the samples were treated with H_2 (100 Torr) for 12 h at r.t., outgassed at r.t. for 1 h and then put into contact with 100 Torr of CO, monitoring the spectra at increasing contact time with CO up to 2 h.

Electron micrographs were obtained by a Jeol 2000EX microscope. Before the introduction in the instrument, the samples, in the form of powders, were ultrasonically dispersed in isopropyl alcohol and a drop of the suspension was deposited on a copper grid covered with a lacey carbon film. Histograms of the particle size distribution were obtained by counting onto the micrographs at least 300 particles; the mean particle diameter (d_m) was calculated by using the formula $d_m = \Sigma d_i n_i / \Sigma n_i$ where n_i was the number of particles of diameter d_i. In the case of metal particles of the Rh/γ-Al_2O_3 (MVS) systems, the diameter d_i used for the calculation in these two cases has been the medium value of each dimensions interval in the histogram, thus with a resulting uncertainty of ± 0.25 nm. The reason for this different data treatment is that rhodium particles in these two cases were very small and the usual mean diameter calculation (where the d_i considered is usually the highest limit of each dimensions interval) lead to an uncertainty of ± 0.5 nm for the mean diameter obtained, and such uncertainty limit was too high for the considered metal particles.

The catalytic samples were prepared for the EXAFS experiments by suspending the fine powders mixed with boron-nitride in ethanol, drying the mixtures under vacuum and pressing them into pellets. The sample amount was calculated in order to achieve a reasonable edge jump of about 0.7.

The EXAFS measurements at the Rh K-edge (23.220 keV) have been performed at the GILDA beamline [7] of the European Synchrotron Radiation Facility (ESRF, Grenoble). The radiation was monochromated and horizontally focused by using a double crystal Si(3 1 1) monochromator [8]; two Pt mirrors were used to reject the higher harmonics and focus the beam in the vertical direction [7].

Two reference samples (α-Rh_2O_3 and Rh foil) and two MVS derived catalysts (Rh/γ-Al_2O_3 and Rh(TOA)/γ-Al_2O_3) were studied, all in transmission mode, using two Ar-filled ionization chambers to detect the incident (I_0) and transmitted (I_T) X-ray beam. The measured absorption coefficient is defined as $\mu(E) = \ln(I_0/I_T)$. All spectra were recorded at 77 K in order to reduce the thermal effects.

The GLC analyses were performed on a Perkin–Elmer Auto System gas chromatograph, equipped with a flame ionization detector (FID), using a SiO_2 column (DB1, 30 m × 0.52 mm, 5 μm) and helium as carrier gas. ^{1}H- and ^{13}C-NMR spectra were measured on Varian Gemini 200 spectrometer at 200 and 50.3 MHz, respectively, using chloroform-*d* as solvent; chemical shifts are relative to internal $Si(CH_3)_4$.

2.2. Preparation of the rhodium catalysts

2.2.1. Synthesis of the solvated Rh atoms

In a typical experiment, rhodium vapour, generated by resistive heating of a tungsten wire surface coated with electrodeposited rhodium (100–150 mg), was co-condensed at liquid nitrogen temperature with mesitylene (40 ml) in the glass reactor chamber of the MVS apparatus in ca. 40 min. The reactor chamber was warmed to the melting point of the solid matrix (ca. −

40 °C) and the resulting brown solution was siphoned at low temperature in a Schlenk tube and kept in a refrigerator at −20 °C. The content of the metal solution was 1.2 mg Rh ml^{-1} (0.0117 mg atom ml^{-1}).

2.2.2. Preparation of rhodium on γ-Al_2O_3 catalysts

The above brown Rh/mesitylene reaction solution (mesitylene-solvated metal atoms) (8.34 ml, 10 mg Rh) was added to a suspension of γ-Al_2O_3 (10 g) in mesitylene (20 ml). The mixture was stirred for 12 h at room temperature. The colourless solution was removed and the light-brown solid, containing 0.1 wt.% Rh, was washed with pentane and dried under reduced pressure. The Rh/γ-Al_2O_3 catalysts, containing 1 and 5 wt.% Rh, were prepared similarly using 1 g and 190 mg of γ-Al_2O_3, respectively.

2.2.3. Preparation of rhodium–trioctylamine (TOA) on γ-Al_2O_3 catalysts

2.2.3.1. Preparation of Rh(TOA)/mesitylene solution. TOA (0.30 ml, 0.69 mmol) was added at the MVS Rh/mesitylene solution (20 ml, 0.23 mg atom) and the mixture was stirred for 1 h at room temperature. The resulting brown Rh(TOA)/mesitylene solution was stable at room temperature for a long time (ca. 3 months).

2.2.3.2. Preparation of the Rh(TOA)/γ-Al_2O_3 catalysts. The brown Rh(TOA)/mesitylene solution (8.34 ml, 10 mg Rh) was added to a suspension of γ-Al_2O_3 (10 g) in mesitylene (20 ml). The mixture was stirred for 12 h at room temperature. The colourless mesitylene was removed and the light-brown solid, containing 0.1 wt.% Rh, was washed with pentane and dried under reduced pressure. The Rh/γ-Al_2O_3 catalysts, containing 1 and 5 wt.% Rh, were prepared similarly using 1 g and 190 mg of γ-Al_2O_3, respectively.

2.3. Catalytic reactions

2.3.1. Hydrogenation of methylbenzoate: general procedure

The hydrogenation experiments were performed at 20 atm starting hydrogen pressure using a 75-ml stainless steel autoclave equipped with a Teflon removable cylinder Jacker, a magnetic bar, a stainless steel tap and a manometer (100 atm end scale). The reactions were performed by heating the autoclave in an oil bath at 80±1 °C. In a typical experiment, the autoclave was charged, under argon atmosphere, with the rhodium catalyst (0.064 mg atom), THF (10 ml) and methylbenzoate (0.8 ml, 6.4 mmol). The autoclave was closed, argon was eliminated and hydrogen was introduced (20 atm). The reaction mixture was stirred (1200 rpm) and heated to 80 °C. The reaction was monitored by GLC analysis of liquid samples removed by the tap. The methyl cyclohexenoate was identified by comparison of its GLC retention time with that of an authentic sample. The conversion as function of the time for different catalysts is reported in Fig. 1.

2.3.2. Hydrogenation of cinnamaldehyde: general procedure

A 50-ml round-bottomed flask was charged with the rhodium catalyst (0.48 mg atom Rh), toluene (15 ml) and cinnamaldehyde (6.1 ml, 48 mmol). The mixture was stirred (ca. 1200 rpm) at room temperature for 12 h. The solution was separated from the catalyst by decantation and analysed by GLC. The products were identified by comparison of their GLC retention times with those of authentic samples. The results obtained using different catalysts are reported in Table 1.

2.3.3. Silylformylation of 1-hexyne: general procedure

The silylformylation experiments were carried out at 10 atm CO starting pressure and room temperature in a 25-ml stainless steel autoclave previously described (see Section 2.3.1). In a typical experiment, the autoclave was charged under argon atmosphere with the rhodium catalyst (0.002 mg atom), toluene (2 ml), dimethylphenylsilane (0.31 ml, 2 mmol) and 1-hexyne (0.23 ml, 2 mmol). The autoclave was closed, argon was eliminated and carbon monoxide was introduced (10 atm). The reaction mixture was stirred (1200 rpm) and monitored by GLC analysis of liquid samples removed by the tap. When silane was completely converted, the autoclave was discharged, pentane (20 ml) was added and the surnatant liquid was separated from the catalyst by decantation. The volatile materials were removed under vacuum and the raw product was recovered by bulb-to-bulb distillation (1 mmHg). Pure (*Z*)-1-(dimethylphenylsilyl)-2-formyl-1-hexene was obtained by column chromatography (silica gel; eluent, pentane:ethylacetate, 95/5) and characterized by ^{1}H- and ^{13}C-NMR [1j].

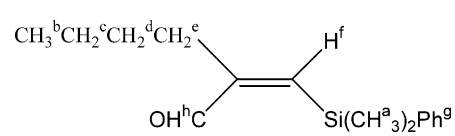

^{1}H-NMR (200 MHz) δ: 0.51 (6H, H^a, s), 0.91 (3H, H^b, t, J^{bc} = 7.0 Hz), 1.22–1.45 (4H, m, H^c, H^d), 2.31 (2H, H^e, t, J^{ed} = 7.3 Hz), 6.93 (1H, H^f, s), 7.35–7.40 (3H, H^g, m), 7.48–7.55 (2H, H^g, m), 9.78 (1H, H^h, s) ppm. ^{13}C-NMR (50.3 MHz) δ: −0.3, 13.7, 22.3, 30.4, 31.4, 128.3, 129.6, 133.7, 137.2, 149.2, 157.4, 193.7 ppm.

The results with different catalysts are reported in Table 2.

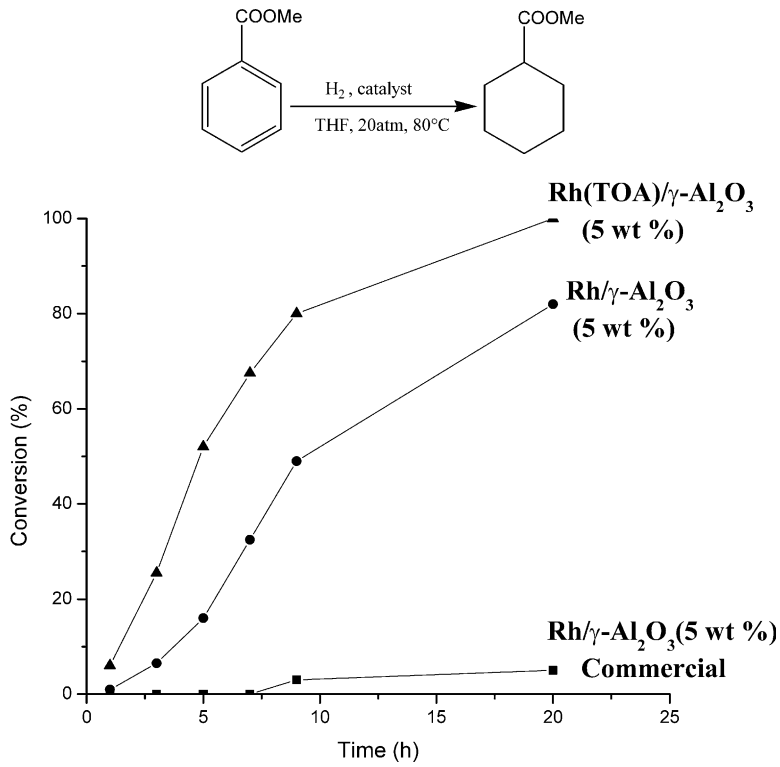

Fig. 1. Hydrogenation of methyl benzoate to methyl cyclohexanoate with rhodium on γ-alumina catalysts.

3. Results and discussion

3.1. Preparation of supported Rh catalysts

The reaction of Rh vapour with mesitylene in large excess, at liquid nitrogen temperature in a reactor elsewhere described [6], affords a reddish-brown matrix which gives, on melting, a brown solution stable at − 40 °C containing mesitylene-stabilized Rh-hydride microclusters [9]. The warming up to room temperature in the presence of supports, such as γ-Al_2O_3, results, by a further clustering process, in a gentle deposition of well-dispersed Rh nanoparticles on the support [10] (Scheme 1).

Table 1
Hydrogenation of cinnamaldehyde with rhodium on γ-Al_2O_3 catalysts [a]

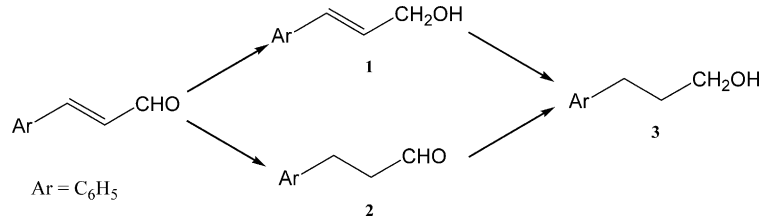

Catalyst	Conversion (%)	Product distribution (%)			
		1	**2**	**3**	Other [b]
Rh/γ-Al_2O_3 (1%)	40	5	60	25	10
Rh/γ-Al_2O_3 (0.1%)	5	25	–	–	75
Rh(TOA)/γ-Al_2O_3 (1%)	82	–	80	10	10
Rh(TOA)/γ-Al_2O_3 (0.1%)	75	–	75	15	10
Rh/γ-Al_2O_3 (5%) commercial	5	10	80	10	–

[a] Reaction conditions: Rh catalyst, 0.48 mg atom; cinnamaldehyde, 6.1 ml (48 mmol); toluene, 15 ml; atmospheric hydrogen pressure; 25 °C; reaction time, 12 h.
[b] Unidentified high boiling products.

Table 2
Silylformylation of 1-hexyne catalyzed by rhodium on γ-Al_2O_3 catalysts

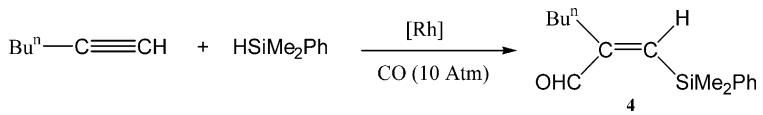

Catalyst	Time (h)	Conversion [a] (%)	(*Z*)-1-(Dimethylphenylsilyl)-2-formyl-1-hexene (%) [b]
Rh/γ-Al_2O_3 (1%)	8	34	100
	24	100	100
Rh(TOA)/γ-Al_2O_3 (1%)	8	72	100
	10	100	100
Rh/γ-Al_2O_3 (5%) commercial	8	–	–

Reaction conditions: Rh catalyst, 0.002 mg atom; toluene, 2 ml; 1-hexyne, 0.23 ml (2 mmol); $PhMe_2SiH$, 0.31 ml (2 mmol); carbon monoxide pressure, 10 atm; 25 °C.
[a] Determined by GLC analysis, based on $PhMe_2SiH$ consumed.
[b] Calculated by GLC analysis.

In the presence of additional stabilizers, such as TOA, the mesitylene-solvated Rh atoms become thermally stable even at room temperature and they can be more easily handled in order to deposit Rh nanoparticles on supports (Scheme 2).

The catalytic activity of the so prepared rhodium systems supported on γ-Al_2O_3 at different Rh loading has been evaluated and compared with that of a commercial Rh/γ-Al_2O_3 sample in some significant reference reactions such as: (i) the hydrogenation of methylbenzoate to methylcyclohexanoate, being this kind of reaction of particular importance in fine chemical syntheses [1n], (ii) the hydrogenation of cinnamaldehyde, an α,β-unsaturated aldehyde very useful to evaluate the chemoselectivity of catalysts [11] and (iii) the silylformylation of 1-hexyne, being the silylformylation of acetylenic compounds a way to produce silylalkenals, useful precursors to polyfunctionalized compounds [12].

3.2. Catalytic reactions of supported rhodium catalysts

3.2.1. Hydrogenation of methyl benzoate

The hydrogenation reaction of methyl benzoate to methyl cyclohexanoate with different catalysts (5 wt.% Rh) has been performed in THF at 80 °C, using a starting hydrogen pressure of 20 atm and a molar ratio substrate:rhodium = 100. The conversion as function of time is reported in Fig. 1.

It can be seen that, under the adopted reaction conditions, the commercial rhodium sample is almost inactive while the MVS-derived rhodium systems are quite efficient catalysts. However, Rh(TOA)/γ-Al_2O_3 is more active than the analogous Rh/γ-Al_2O_3 prepared in the absence of the stabilizer.

3.2.2. Hydrogenation of cinnamaldehyde

The hydrogenation of cinnamaldehyde has been performed at room temperature under atmospheric pressure of H_2 using Rh/γ-Al_2O_3 and Rh(TOA)/γ-Al_2O_3 catalysts with Rh loadings in the range 0.1–1%, lower than those generally required for the hydrogenation of aromatic rings ($\geq$5%) [13]. The products, formed in this reaction, are 3-phenylpropanal (**1**) and the cinnamyl alcohol (**2**) deriving from the hydrogenation of the double bond and the carbonyl group, respectively, and the 3-phenyl-1-propanol (**3**) as final product of the reduction. The results obtained are summarized in Table 1.

It appears from the reported data that the Rh(TOA)/γ-Al_2O_3 catalyst is largely more active than the analogous sample prepared in the absence of TOA as additional stabilizer. Such a difference is much more evident at very low Rh loading (0.1%) where the Rh(TOA)/γ-Al_2O_3 catalyst shows a still good activity,

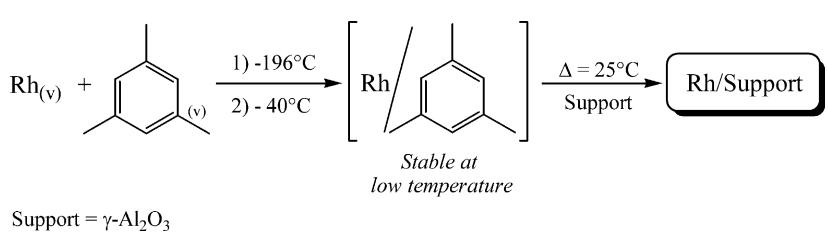

Scheme 1.

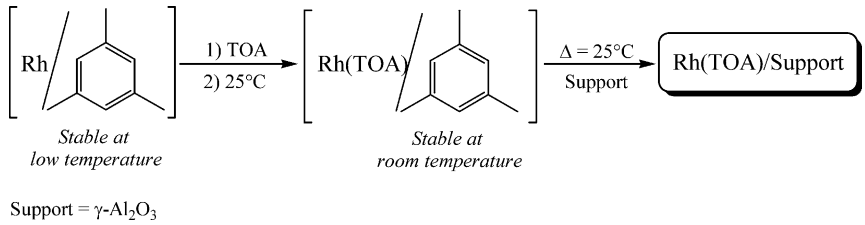

Scheme 2.

while the Rh/γ-Al_2O_3 system is quite inactive. Under the adopted reaction conditions, the commercial Rh/γ-Al_2O_3 sample is a very poor catalyst. With the exception of the 0.1 wt.% Rh/γ-Al_2O_3 system, where high boiling unidentified compounds are formed as main products, all the catalysts show a quite good chemoselectivity in the hydrogenation of cinnamaldehyde to 3-phenylpropanal (**2**).

3.2.3. Silylformylation of 1-hexyne

The silylformylation of acetylenes is an important reaction widely studied using homogeneous Rh catalytic precursors [1j,14] and no examples are reported in the literature on silylformylation performed using rhodium-based heterogeneous catalysts. In general, the reaction with 1-alkynes gives (*Z*)-3-silyl-2-alkenals (**4**) as main products, although minor amounts of other products, deriving from hydrosilylation, **5**, and silylformylation–hydrosilylation reactions, **6** and **7**, can be detected (Scheme 3).

The results obtained in the silylformylation of 1-hexyne with CO and dimethylphenylsilane using different heterogeneous rhodium on γ-Al_2O_3 catalysts are reported in Table 2.

The reaction in the presence of the Rh vapour derived catalysts proceeds with total regio- and stereoselectivity giving (*Z*)-1-(dimethylphenylsilyl)-2-formyl-1-hexene as the sole product, being the Rh(TOA)/γ-Al_2O_3 system largely more active than the analogous one without TOA, as also observed in the previously described hydrogenation reactions. It is noteworthy that the commercial Rh/γ-Al_2O_3 sample is completely inactive under the adopted reaction conditions.

3.3. Structural studies of supported rhodium catalysts

In order to rationalize the different behaviour of the Rh catalysts employed, IR studies of adsorbed CO species, HRTEM and EXAFS analyses have been performed on the Rh vapour derived systems Rh/γ-Al_2O_3 and Rh(TOA)/γ-Al_2O_3 as well as on the commercial Rh/γ-Al_2O_3 sample (except EXAFS).

3.3.1. IR studies of adsorbed CO

FTIR spectroscopy of adsorbed CO is usually employed to investigate the surface properties of supported metal particles because of the high sensitivity of the vibrational characteristics of the surface carbonylic adducts towards the adsorbing sites properties [1d,15–18]. In this section, the IR spectra of CO adsorbed on the Rh/γ-Al_2O_3 catalysts considered, two prepared via MVS and a commercial one, will be discussed.

Before the admission of CO, the samples were put into contact with 100 Torr H_2 and then outgassed at room temperature. These conditions were adopted to obtain information about the surface properties of the small metal particles in a condition proximal to one in which they were produced and employed as catalysts [19].

3.3.1.1. IR spectra of CO adsorbed on commercial Rh/γ-Al_2O_3. In the case of Rh/γ-Al_2O_3 commercial sample, the spectrum obtained immediately after admission of CO shows a main peak at 2065 cm^{-1} with a shoulder at ca. 2086 cm^{-1}, a partially resolved component at 2012 cm^{-1} and a band centred at 1870 cm^{-1} (Fig. 2a). By increasing the contact time with CO up to 2 h (Fig. 2b–

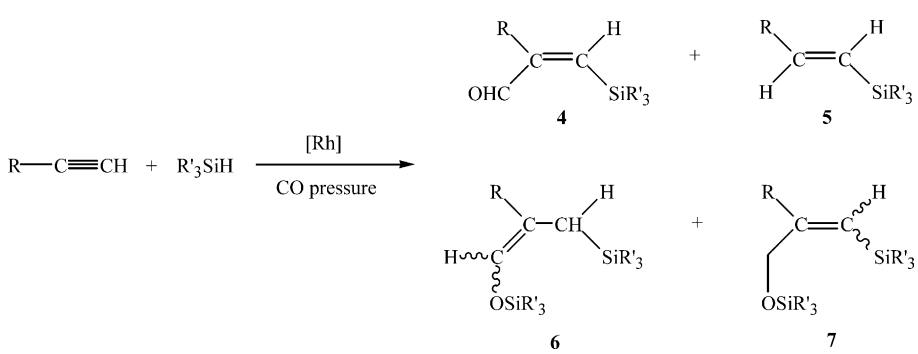

Scheme 3.

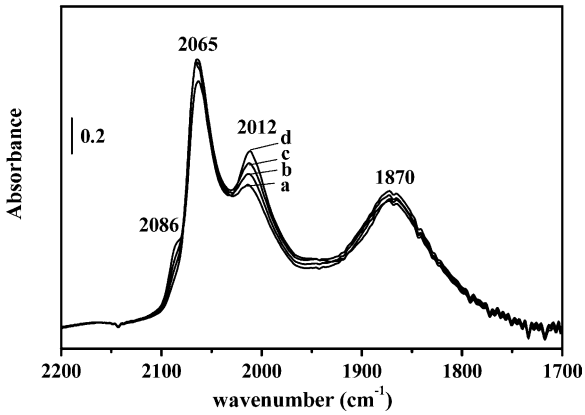

Fig. 2. IR spectra of CO (100 Torr) adsorbed on the commercial Rh/γ-Al_2O_3 (5 wt.% Rh) sample: (a) immediately after CO adsorption; (b) after 5 min; (c) after 20 min; (d) after 2 h of contact with CO.

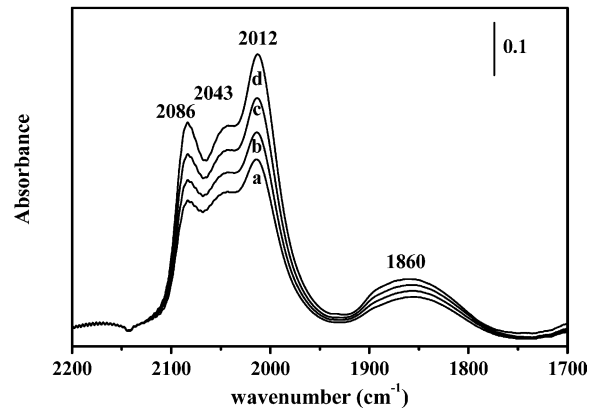

Fig. 3. IR spectra of CO (100 Torr) adsorbed on the Rh/γ-Al_2O_3 (MVS) (1 wt.% Rh) sample: (a) immediately after CO adsorption; (b) after 5 min; (c) after 20 min; (d) after 2 h of contact with CO.

d), the intensity of the signals at 2086 and 2012 cm^{-1} progressively increases. On the contrary, the intensity of the bands at 2065 cm^{-1} slightly decreases and the one at 1870 cm^{-1} remain nearly unchanged.

By using a band fitting program, the components at 2086 and 2012 cm^{-1} were extracted from the experimental profile, and their integrated intensities were calculated. The ratio between the intensity at increasing time of contact with CO (I_t) and the intensity exhibited immediately after CO adsorption (I_0) was found to be the same for both components, indicating that they are the same chemical species and, precisely, dicarbonyls on Rh(I) [20–23]. The formation of $Rh(I)(CO)_2$ species by interaction of CO with Rh(0) particles has been already observed in previous works and explained in terms of a process occurring through the following steps: (i) CO adsorption on Rh(0) atoms at the surface of rhodium particles; (ii) extraction of such Rh(0) atoms from the surface by formation of a volatile rhodium carbonyl (the exact stoichiometry of which is not known yet); (iii) migration of the volatile Rh(0) carbonyls to the support, the hydroxyls of which oxidize the metal atoms to Rh(I), with the consequent formation of H_2.

Concerning the band at 2065 and 1870 cm^{-1}, the first can be assigned to the stretching mode of monocarbonyls linearly adsorbed on Rh(0) particles [24–26], and the second is due to carbonyls adsorbed in bridged form on pairs of rhodium atoms [20–22].

3.3.1.2. IR spectra of CO adsorbed on Rh/Al_2O_3 (MVS). Also the spectral pattern obtained by contacting CO with the Rh/γ-Al_2O_3 (MVS) sample exhibited components due to monocarbonyls (both linear and bridged) on metal particles and Rh(I) dicarbonyls coming from the erosion of rhodium atoms. However, significant differences in relative intensity compared to commercial sample are evident. In fact, in the spectra recorded immediately after CO admission at different times (Fig. 3), the bands at 2086 and 2012 cm^{-1} due to $Rh(I)(CO)_2$ species were more intense as compared to ones observed for the commercial sample (Fig. 2) while the components due to linear (2043 cm^{-1}) and bridged (broad and complex, in the 1900–1800 cm^{-1} range) Rh(0) carbonyls were observed as minor components.

The predominance of the components due to $Rh(I)(CO)_2$ species indicates that the metal particles in this MVS sample exhibit a high number of surface metal atoms in low coordination, which are those more easily extracted by CO to form the volatile Rh(0) carbonyls, precursors of the Rh(I) dicarbonyls. This fact is in agreement with the small size of the metal particles of the Rh/Al_2O_3 (MVS) sample evidenced by TEM (see Fig. 5), as the number of surface atoms in low coordination on corners and edge is expected to increase as the size of metal particles decreases [27].

3.3.1.3. IR spectra of CO adsorbed on Rh(TOA)/γ-Al_2O_3 (MVS). The spectral pattern following CO

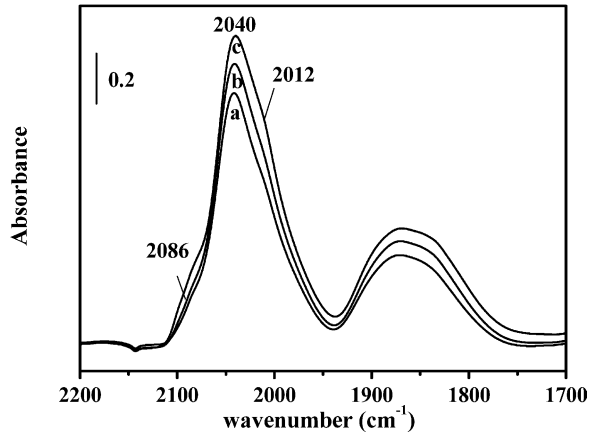

Fig. 4. IR spectra of CO (100 Torr) adsorbed on the Rh(TOA)/γ-Al_2O_3 (MVS) (1 wt.% Rh) sample: (a) immediately after CO adsorption; (b) after 5 min; (c) after 20 min; (d) after 2 h of contact with CO.

admission on Rh(TOA)/γ-Al_2O_3 (MVS) was found to be different from previous samples, in terms of relative intensity and evolution during the time of the bands due to the Rh(0) and Rh(I) carbonyls (Fig. 4). The spectrum recorded immediately after admission of CO onto the sample (Fig. 4a) showed as main components a band at 2043 cm^{-1} and the broad absorption in the 1900–1800 cm^{-1} range due to linear and bridged monocarbonyls on Rh(0) at the surface of metal particles, respectively. The signals at 2086 and 2012 cm^{-1}, due to Rh(I)$(CO)_2$ species, resulting from the surface erosion of the metal particles, appeared just as two very weak shoulders of the peak at 2043 cm^{-1} (Fig. 4a), in sharp contrast with the situation of Rh/γ-Al_2O_3 (MVS) where they were by far the dominant peaks (Fig. 3).

By prolonging the contact time with CO (Fig. 4b and c), even if the shoulders at 2086 and 2012 cm^{-1} appeared slightly more pronounced, the mean spectroscopic features are those related to carbonyls on Rh(0).

This result appears quite surprising as considering that analysis TEM showed that in the Rh(TOA)/γ-Al_2O_3 (MVS) sample, the metal particles are smaller than the Rh/γ-Al_2O_3 (MVS) one (see Section 3.3.2), and then they should expose at their surface an even higher number of Rh atoms in low coordination, easily abstracted by CO to form Rh(I)$(CO)_2$ species stabilized on the support. It can be supposed that the inertness towards this process exhibited by the metal particles of the Rh(TOA)/γ-Al_2O_3 (MVS) sample resulted from the presence of TOA molecules. As the nitrogen is a donor atom, it could stabilize in some entity the Rh sites slowing down the process of surface erosion.

3.3.2. High-resolution transmission electron microscopy (HRTEM) studies

The metal particle size distribution studied by HRTEM of the commercial Rh/γ-Al_2O_3 (5 wt.% Rh) system (Fig. 5, A1) shows the presence of metal particles with a broad size distribution lying in the 1.5–14 nm range, with a resulting average diameter of 7.0 ± 0.5 nm (Fig. 5, B1).

The HRTEM analysis of the Rh/γ-Al_2O_3 (MVS) catalyst (micrograph shown in Fig. 5, A2) indicated the presence of supported rhodium particles smaller than the commercial sample, having a size distribution in a narrow range, 1.0–4.0 nm, and a mean diameter $d_m = 2.1 \pm 0.25$ nm (Fig. 5, B2). In this case, moreover, two additional indications has to be considered: the former is that HRTEM has not an high sensitivity in revealing particles smaller than 1 nm in size, and the latter is that the occurrence of aggregation phenomena of sub-nanometric metal particles under the electron beam during HRTEM observation cannot be excluded [28]. So, as observed in previous studies [29], the real mean size of Rh particles could be even smaller.

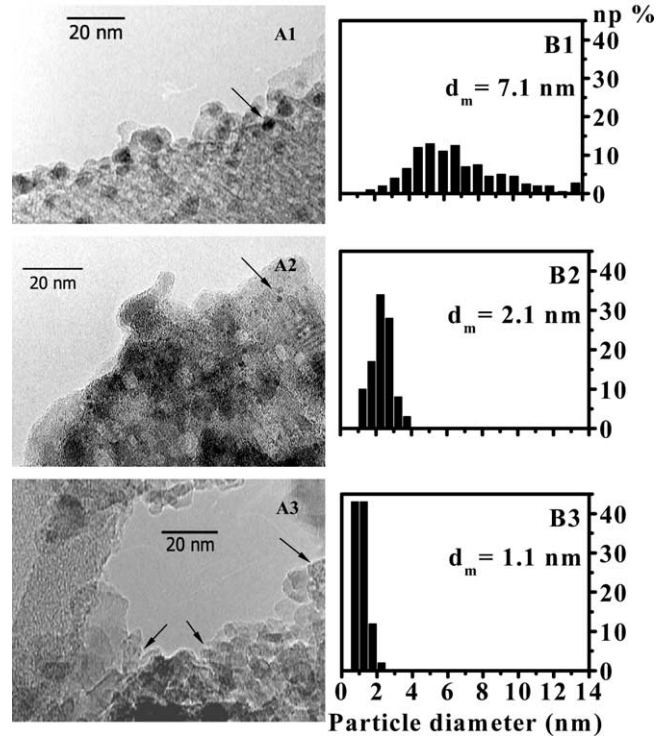

Fig. 5. Section A: Electron micrographs (original magnification 200,000 ×) of commercial Rh/γ-Al_2O_3 (A1), Rh/γ-Al_2O_3 (MVS) (A2) and Rh(TOA)/γ-Al_2O_3 (MVS) (A3). Section B: Histograms of the particle size distribution of the samples: commercial Rh/γ-Al_2O_3 (B1); Rh/γ-Al_2O_3 (MVS) (B2); Rh(TOA)/γ-Al_2O_3 (MVS) (B3).

Concerning the Rh(TOA)/γ-Al_2O_3 (MVS) system (micrograph in Fig. 5, A3), the metal particle size distribution of the supported metallic phase, reported in Fig. 5, B3, appeared further shifted to smaller diameters, with the resulting mean diameter $d_m = 1.1 \pm 0.25$ nm. Such a distribution is highly asymmetric and the maximum corresponds to the smallest particle size detectable by HRTEM. This feature allows us to suggest the presence of rhodium particles even smaller. In the end, the presence of a nucleophilic stabilizer such as TOA during the MVS synthesis, as indicated by the data obtained, yielded the formation of the smallest metal particles.

3.3.3. EXAFS studies on the MVS derived catalysts

The EXAFS data have been analysed using the GNXAS package which allows deconvolutions of the contributions to the EXAFS signal, due to the local atomic arrangement around the absorbing atom, in terms of irreducible n-body contributions, $\gamma^{(n)}$ [30,31]. The EXAFS data analysis by GNXAS has been applied, as first, to the two reference samples: α-Rh_2O_3 and Rh foil. In Fig. 6, the best-fit results obtained on the total EXAFS signals and their residuals are reported. The structural results obtained by the curve-fitting procedures are reported in Table 3. The values found for the reference samples are in good agreement with the

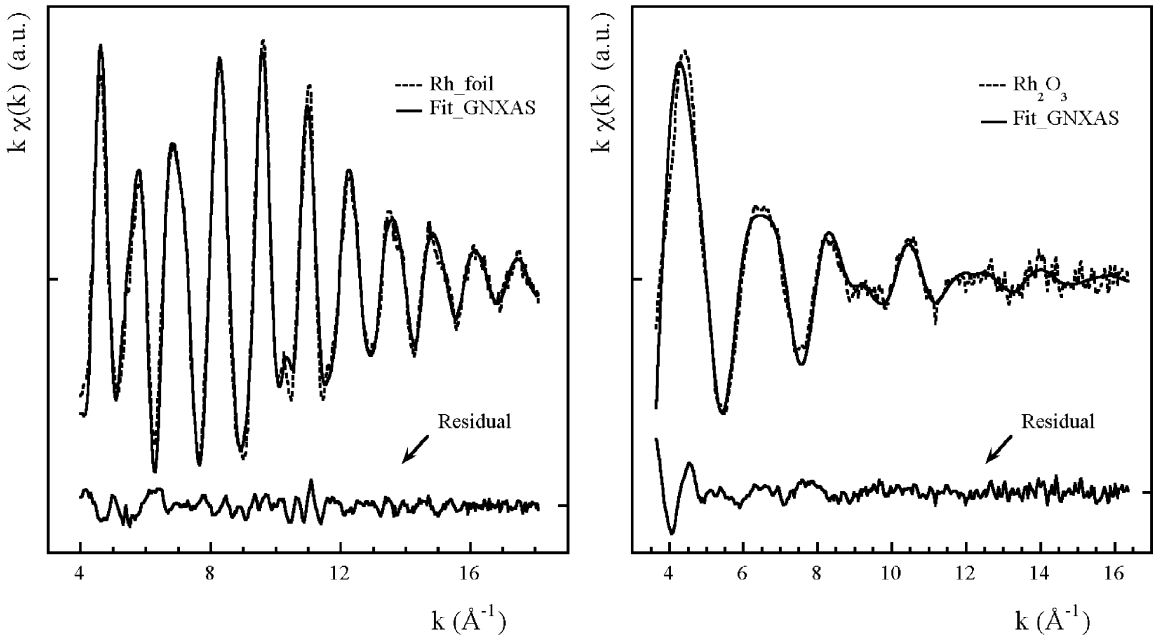

Fig. 6. Best-fit results for Rh foil (left panel) and Rh_2O_3 (right panel).

expected ones and this allowed us to use the same local potentials to generate the $\gamma^{(n)}$ contributions for the EXAFS signals of the two catalytic samples.

The experimental k-weighted EXAFS signal of rhodium oxide was well reproduced using only three single scattering contributions, $\gamma^{(2)}$, related to the first Rh–O, the second Rh–Rh and the third Rh–O coordination shells. In agreement with the analysis previously reported [32], the rhodium foil required three $\gamma^{(2)}$ due to the first three Rh–Rh coordination shells but also a $\gamma^{(3)}$ due to the focussing effect which enhances the multiple scattering contribution to the fourth FCC shell.

The k-weighted Fourier transforms (FTs) of the $\chi(k)$ spectra of the two reference samples and of the two MVS derived catalysts, Rh/γ-Al_2O_3 and Rh(TOA)/γ-Al_2O_3, are reported in Fig. 7.

The FT of Rh_2O_3 shows only two main peaks, the first relative to the Rh–O first shell distance while the second includes two contributions (Rh–Rh and Rh–O). The Rh foil FT spectrum is typical of an FCC structure and the first four Rh–Rh contributions are clearly visible.

The Fourier transforms of the two catalysts are quite different. They present two main peaks that, by comparison with the model compound spectra, can be qualitatively assigned to a metal–oxygen or metal–light atom coordination and to a metal–metal coordination, to form small Rh clusters. The analysis and the

Table 3
EXAFS structural parameters obtained fitting the reference samples (α-Rh_2O_3 and Rh foil) and the Rh/γ-Al_2O_3 sample taking into account an oxide and a metal phase

Oxide phase	α-Rh_2O_3	Rh/Al_2O_3	Metal phase	Rh-foil	Rh/Al_2O_3
N_{Rh-O}	6.0 (0.3)	2.7 (0.3)	N_1	12.0 (0.3)	4.0 (0.3)
R_{Rh-O} (Å)	2.04 (0.02)	2.05 (0.02)	R_1 (Å)	2.68 (0.01)	2.69 (0.02)
σ^2_{Rh-O} (10^{-3} Å^2)	3.0 (0.2)	1.3 (0.2)	$^2_1$ (10^{-3} Å^2)	2.8 (0.2)	5.0 (0.2)
N_{Rh-Rh}	3.0 (0.2)	0.9 (0.2)	N_2	6.0 (0.2)	1.8 (0.2)
R_{Rh-Rh} (Å)	3.01 (0.03)	3.01 (0.03)	R_2 (Å)	3.80 (0.01)	3.80 (0.02)
σ^2_{Rh-Rh}(10^{-3} Å^2)	9.0 (0.2)	9.8 (0.2)	$^2_2$ (10^{-3} Å^2)	2.8 (0.2)	7.6 (0.3)
N_{Rh-O}	3.0 (0.2)	1.2 (0.3)	N_3	24.0 (0.4)	5.5 (0.3)
R_{Rh-O} (Å)	3.47 (0.03)	3.47 (0.03)	R_3 (Å)	4.67 (0.01)	4.69 (0.02)
σ^2_{Rh-O} (10^{-3} Å^2)	20.0 (0.2)	14.0 (0.2)	$^2_3$ (10^{-3} Å^2)	7.5 (0.3)	8.0 (0.3)
			N_4	12.0 (0.3)	–
			R_4 (Å)	5.36 (0.02)	5.37 (0.03)
			$^2_4$ (10^{-3} Å^2)	5.7 (0.2)	9.4 (0.3)
			θ (°)	178 (2.0)	183 (3.0)

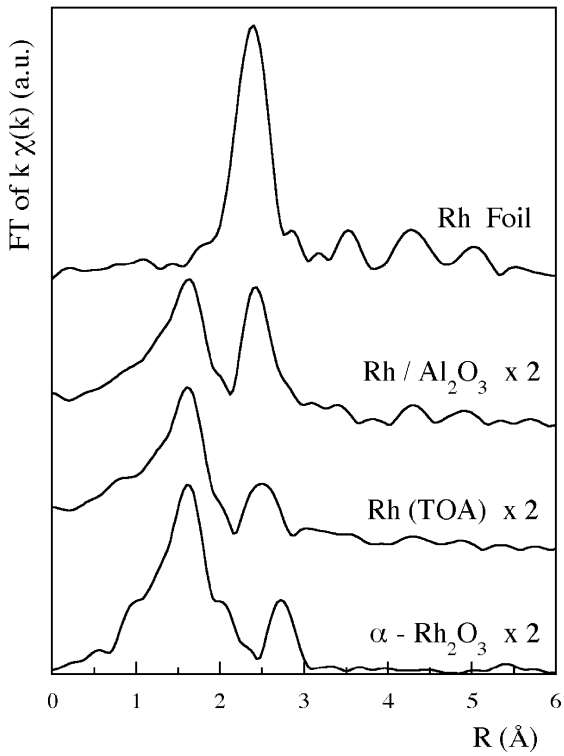

Fig. 7. Fourier transforms, FTs, of the EXAFS data of the reference samples (Rh foil and Rh_2O_3) and of the two MVS derived catalysts Rh/γ-Al_2O_3 and Rh(TOA)/γ-Al_2O_3.

interpretation of the spectra of both catalytic samples is complicated by the presence of Rh atoms in these two different phases. In Figs. 8 and 9, the comparison between best-fit of the EXAFS spectra and of the FTs of the two catalysts are shown.

In the case of Rh/γ-Al_2O_3 sample, the Rh atoms are present in two different states: oxide and metal. In fact best-fit of the data was achieved with the contribution of first three coordination shells coming from Rh_2O_3 and four Rh–Rh contributions characteristic of metallic rhodium. As reported in Table 3, the interatomic distances found are in agreement with the ones of the reference samples.

For the analysis of the EXAFS data of the Rh(TOA)/γ-Al_2O_3 sample, different procedures were used. As first a situation similar to the one found for the Rh/Al_2O_3 catalyst was taken into account (see Fig. 9) and the results achieved are reported in Table 4.

In this case, the interatomic distances found for the second and third shell of the oxide contribution are different from the α-Rh_2O_3 ones, while there is a good agreement for what concerns the metal contributions. We conclude that in this case the Rh is not coordinated as in the α-Rh_2O_3 oxide phase. It has been well proved that in unsupported metal particles stabilized by surfactants, the stabilizer surrounds the metal as a protective layer [1b,1d,32]; on supported samples although very few data are at the moment available, it seem reasonable to suppose that the stabilizer should still cover the metal particles [1d]. Considering this, a new fitting procedure was applied assuming a model composed of a metal phase plus two contributions: Rh–N and Rh–C. The best-fit parameters are reported in Table 5 while Fig. 10 shows the comparison between the FTs of the best-fit of the theoretical model data and of the experimental data.

The good agreement between a theoretical model, in which the surfactants surround the metal particles, and the experimental data shows that this model is acceptable. However, it is not possible to exclude the presence of other light atoms as nearest neighbours.

Further information can be achieved by EXAFS data concerning the size of the metallic clusters. Since Rh is present in two different phases, bound to other Rh

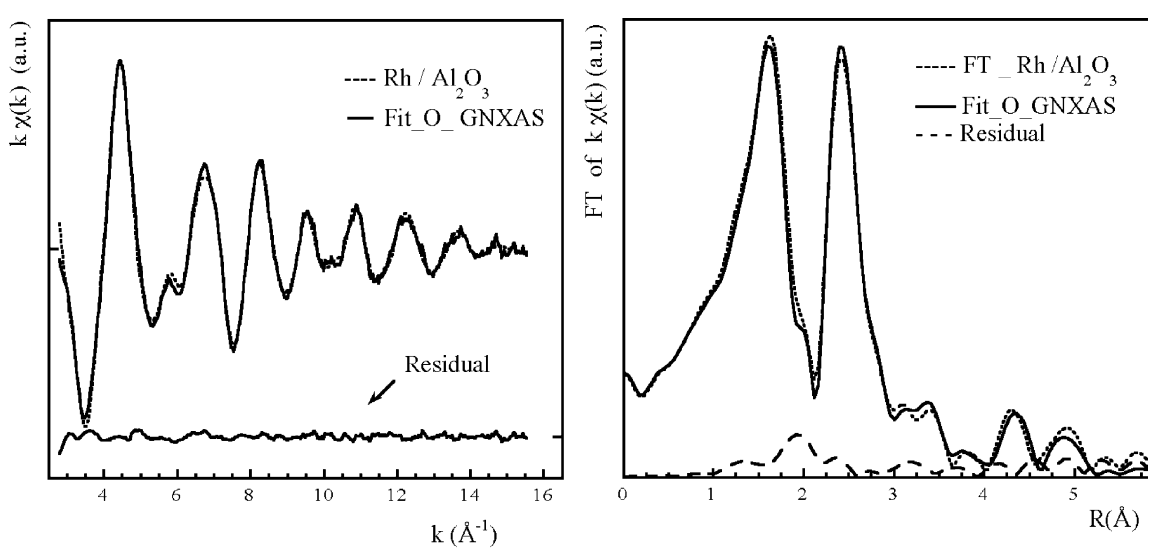

Fig. 8. The left panels show the experimental $k\chi(k)$ data (dots) and the best-fit (full line) while the right panels show the comparison of the Fourier transforms of the $k\chi(k)$ of the MVS Rh/γ-Al_2O_3 catalyst (best-fit is the full line).

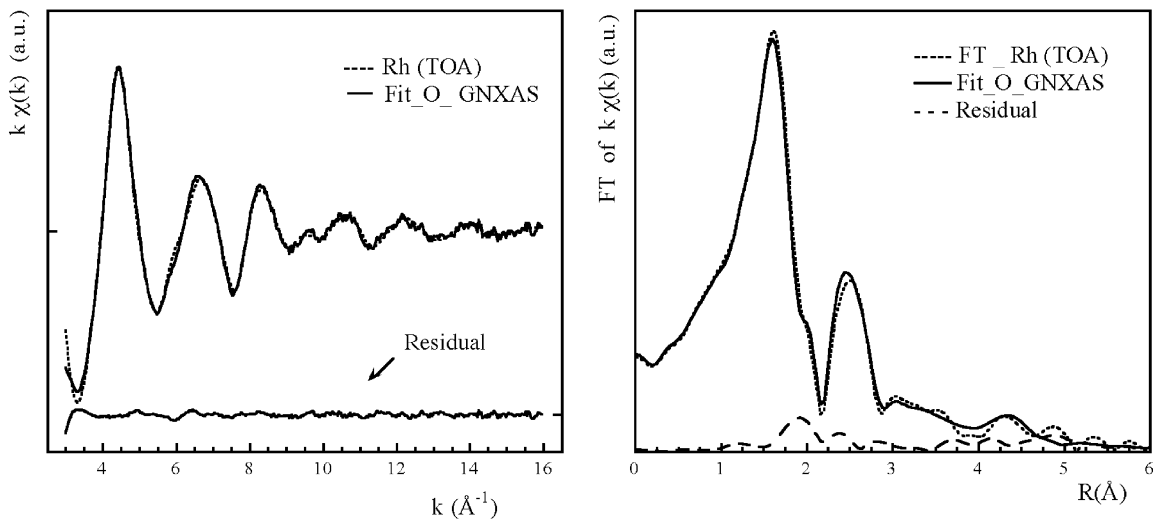

Fig. 9. The left panels show the experimental $k\chi(k)$ data (dots) and the best-fit (full line) while the right panels show the comparison of the Fourier transforms of the $k\chi(k)$ of the MVS Rh(TOA)/γ-Al_2O_3 catalyst (best-fit is the full line).

Table 4
EXAFS structural parameters obtained fitting Rh (TOA)/γ-Al_2O_3 sample taking into account an oxide and a metal phase

Oxide phase	Rh (TOA)/ Al_2O_3_O	Metal phase	Rh (TOA)/ Al_2O_3
N_{Rh-O}	3.4 (0.3)	N_1	2.3 (0.2)
R_{Rh-O} (Å)	2.05 (0.02)	R_1 (Å)	2.69 (0.02)
σ^2_{Rh-O} (10^{-3} Å^2)	1.9 (0.2)	σ^2_1 (10^{-3} Å^2)	8.8 (0.3)
N_{Rh-Rh}	0.4 (0.1)	N_2	1.2 (0.2)
R_{Rh-Rh} (Å)	3.07 (0.04)	R_2 (Å)	3.80 (0.03)
σ^2_{Rh-Rh}(10^{-3} Å^2)	2.0 (0.4)	σ^2_2 (10^{-3} Å^2)	15.3 (0.3)
N_{Rh-O}	2.9 (0.2)	N_3	3.0 (0.3)
R_{Rh-O} (Å)	3.22 (0.04)	R_3 (Å)	4.70 (0.04)
σ^2_{Rh-O} (10^{-3} Å^2)	2.5 (0.3)	σ^2_2 (10^{-3} Å^2)	13.0 (0.4)

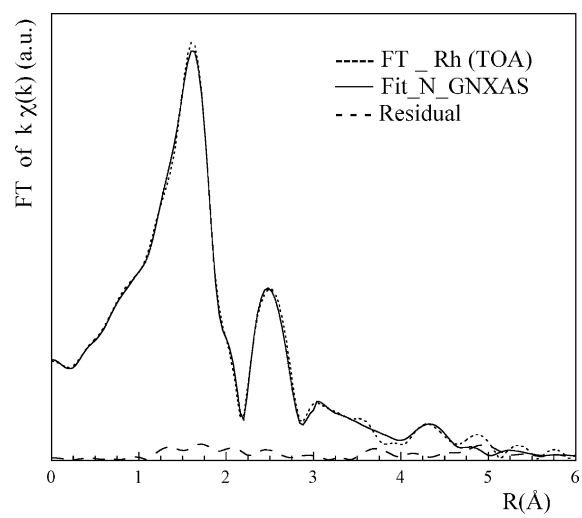

Fig. 10. Comparison of the Fourier transforms of the $k\chi(k)$ of the MVS Rh(TOA)/γ-Al_2O_3 catalyst (best-fit is the full line) and of the theoretical model including N.

Table 5
EXAFS structural parameters obtained fitting Rh(TOA)/γ-Al_2O_3 with a theoretical model that includes only two light elements contributions (Rh–N and Rh–C) and a metal phase

	Rh (TOA)/ Al_2O_3_N	Metal phase	Rh (TOA)/ Al_2O_3
N_{Rh-N}	3.7 (0.3)	N_1	2.6 (0.3)
R_{Rh-N} (Å)	2.07 (0.02)	R_1 (Å)	2.70 (0.02)
σ^2_{Rh-N} (10^{-3} Å^2)	3.2 (0.2)	σ^2_1 (10^{-3} Å^2)	10.5 (0.3)
		N_2	1.1 (0.2)
		R_2 (Å)	3.80 (0.03)
		σ^2_2 (10^{-3} Å^2)	18.4 (0.3)
N_{Rh-C}	2.8 (0.2)	N_3	2.9 (0.3)
R_{Rh-C} (Å)	3.24 (0.04)	R_3 (Å)	4.70 (0.04)
σ^2_{Rh-C} (10^{-3} Å^2)	3.1 (0.3)	σ^2_2 (10^{-3} Å^2)	16.5 (0.4)

atoms and to light backscattering atoms, it is not possible to deduce the Rh cluster dimensions in a simple way, from the coordination numbers (N), as usually done. In this case, in fact, as shown elsewhere [33], the N values found are not the real coordination numbers (N_{th}) but are weighted by the atomic percentage (α) of Rh atoms present in the metallic phases, i.e. $N = \alpha N_{th}$.

Because the atomic percentage, α, is not known, we calculated the expected theoretical mean coordination numbers for the first three coordination shells assuming clusters of a spherical shape with an FCC structure and radius R_c. Dividing the experimental N values by the calculated ones, we obtain three estimations of α as a function of the cluster radius, R_c, one from each coordination shell.

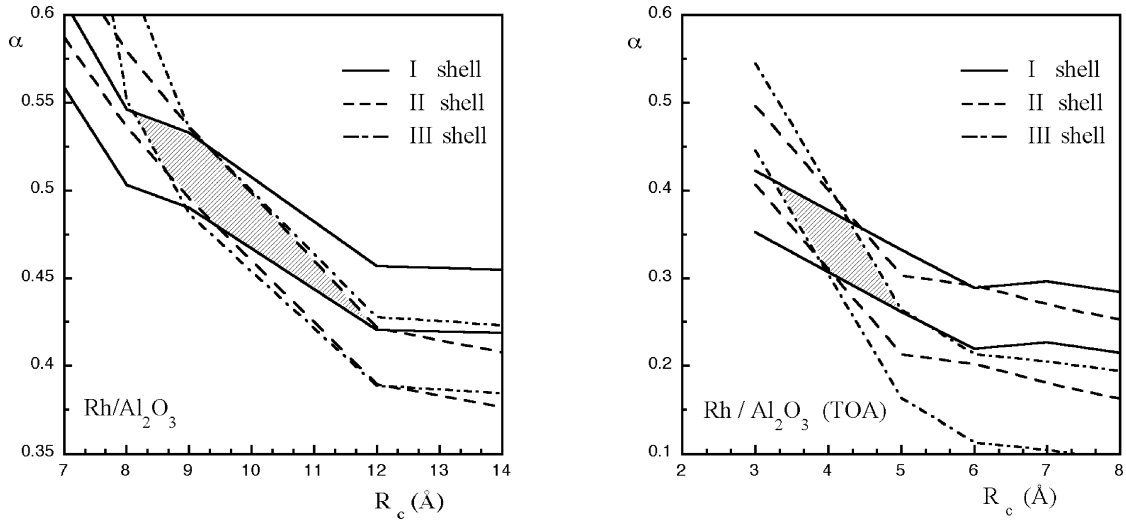

Fig. 11. Ratio, α, of the experimental and theoretical N values for the Rh/γ-Al_2O_3 and the MVS Rh(TOA)/γ-Al_2O_3 samples drawn as a function of the cluster radius, R_c.

Apart from statistical errors, the three curves obtained should intersect at an R_c value that represents the actual cluster dimension. From a more realistic point of view, taking into account the errors, for each shell two curves are obtained that do not define a point but an overlap region whose R_c range gives an estimation of the possible metallic cluster dimension (Fig. 11). For Rh/Al_2O_3 sample, the overlap region is in the range 8.0 Å $< R_c <$ 11 Å while for the Rh(TOA)/γ-Al_2O_3 sample, the overlap region is in the range 3.5 Å $< R_c <$ 5 Å. The mean diameters so determined are: D19 Å for Rh/γ-Al_2O_3 and D8 Å for Rh(TOA)/γ-Al_2O_3.

The mean diameters found using EXAFS are in both cases smaller than those found with HRTEM. As already underlined [29,34] in the presence of a cluster size distribution, EXAFS measures an average dimension weighted by the fraction of atoms corresponding to all the different sizes. For this reason, we can conclude that in both samples there is a large amount of Rh atoms in particles with dimensions smaller than 10 Å, which are clearly visible by EXAFS but are not seen by HRTEM and that the average dimensions of the clusters is lower in the presence of TOA than in its absence. It seems that the main effect of TOA is to prevent the aggregation of atoms/clusters to form larger particles. It can be due to the presence of a protective layer around the metal core, which avoids direct metal–metal contacts.

4. Conclusions

The results obtained in some important reference reactions, as the hydrogenation of methyl benzoate and cinnamaldehyde and the silylformylation of 1-hexyne, have evidenced a quite different catalytic activity of the Rh/γ-Al_2O_3 samples. The Rh/γ-Al_2O_3 commercial catalyst shows, under the adopted reaction conditions, a poor catalytic activity, while the Rh(TOA)/γ-Al_2O_3 sample, prepared from mesitylene-solvated Rh atoms, stabilized by TOA, is a very efficient catalyst, resulting also more active than the analogous Rh/γ-Al_2O_3 sample prepared in the absence of TOA.

The structural characterization of the above catalysts satisfactory accounts of this different behaviour. The IR spectrum detected after treatment with CO of the Rh/γ-Al_2O_3 commercial sample shows peaks consistent with the presence of Rh(I) and Rh(0) carbonyl species. In the MVS Rh/γ-Al_2O_3 derived catalyst, the components due to the Rh(I) carbonyls are predominant; this result agrees with the presence of small rhodium metal particles from which rhodium atoms can be easily extracted to form the volatile Rh(0) carbonyl precursors of Rh(I) species (vide infra). The HRTEM data are consistent with this finding showing the presence of metal particles averaging 7.0 nm in the commercial sample and 2.1 nm in the Rh/γ-Al_2O_3 catalyst.

The IR spectrum following CO admission on Rh(TOA)/γ-Al_2O_3 catalyst is really different from those of the previous sample. It shows as main component only bands due to Rh(0) species. This is quite surprising considering that HRTEM analysis indicates the presence of very small Rh clusters, averaging 1.1 nm in diameter which should have more rhodium atoms easily attacked by CO to form Rh(I) carbonyl species. It is then reasonable to suppose that TOA still surrounds the metal clusters deposited on γ-Al_2O_3 avoiding surface erosion.

The EXAFS study strongly supports this hypothesis. The Fourier transforms of the EXAFS data of the two MVS derived catalysts, Rh/γ-Al_2O_3 and Rh(TOA)/γ-Al_2O_3, are quite different. While in the Rh/γ-Al_2O_3

sample, the Rh atoms are present in two different states, that is as oxide and as metal, in the Rh(TOA)/γ-Al_2O_3 sample the Rh atoms are not present as an oxide phase and the experiment data are in good agreement with a theoretical model composed of a metal phase plus a contribution due to the presence of the amine and attributed to Rh–N or Rh–C interactions.

The enhanced activity of the Rh(TOA)/γ-Al_2O_3 catalyst can be then reasonably related with these factors. In fact, the presence of homogeneously distributed metal particles of largely small size makes available more rhodium atoms for the catalysis. In addition, the stabilization action of TOA on the particles prevents poisoning and an extensive oxidation by the solid oxide support. They can also satisfactorily explain why catalysts at very low Rh loading (0.1%) are still active in the hydrogenation of cinnamaldehyde only when prepared in the presence of TOA (Table 1).

These catalysts can be used several times without valuable lost of activity. In preliminary experiments, it has been observed that hexadecylamine and trioctylaminomethylamonium bromide behave like TOA, while, using polyvinylpyrrolidone, the resulting catalyst exhibit a quite low activity, probably because of a more difficult access of substrates to the metal surface.

Acknowledgements

We gratefully acknowledge financial supports by CNR, Italy (PF-MSTA II) and MIUR, Italy (low 95/95).

References

[1] (a) K.J. Klabunde, Free Atoms, Clusters and Nanoscale Particles, Accademic Press, New York, 1994;
(b) N. Nasar, F. Fache, M. Lemaire, J.-C. Beziat, M. Besson, P. Gallezot, J. Mol. Catal. 87 (1994) 107;
(c) G. Vitulli, A. Verrazzani, A.M. Caporusso, E. Pitzalis, P. Pertici, P. Salvadori, in: S. Daolio, E. Tondello, P.F. Vigato (Eds.), Syntheses and Methodologies in Inorganic Chemistry: New Compounds and Materials, vol. 7, La Photograph, Padova, 1997, p. 52;
(d) H. Bönnemann, G. Braun, W. Brijoux, R. Brinkmann, A. Schulze Tilling, K. Seevogel, K. Siepen, J. Organomet. Chem. 520 (1996) 143;
(e) Y. Wang, H. Liu, N. Toshima, J. Phys. Chem. 100 (1996) 19533;
(f) G. Vitulli, E. Pitzalis, A. Verrazzani, P. Pertici, P. Salvadori, G. Martra, Mat. Sci. Forum 929 (1997) 235;
(g) K.S. Weddle, J. Aiken, III, R.G. Finke, J. Am. Chem. Soc. 120 (1998) 5653;
(h) N. Toshima, T. Yonazawa, New J. Chem. 22 (1998) 1179;
(i) J. Schulz, A. Roucoux, H. Patin, JCS Chem. Commun. (1999) 535.;
(j) N. Toshima, Y. Shiraishi, T. Teranishi, M. Miyake, T. Tominaga, H. Watanabe, W. Brijoux, H. Bönnemann, G. Schmid, Appl. Organomet. Chem. 15 (2001) 178;
(k) H. Bönnemann, R. Richards, Eur. J. Inorg. Chem. (2001) 2455.;
(l) L.A. Aronica, S. Terreni, A.M. Caporusso, P. Salvadori, Eur. J. Org. Chem. (2001) 4321.;
(m) G. Vitulli, M. Bernini, S. Bertozzi, E Pitzalis, P. Salvadori, S. Coluccia, G. Martra, Chem. Mater. 14 (2002) 1183;
(n) J.A. Widegren, R.G. Finke, J. Mol. Catal. A 191 (2003) 187.
[2] (a) See as examples: S. Abbet, A. Sanchez, U. Heiz, W.-D. Schneider, A.M. Ferrari, G. Pacchioni, N.Rosch, J. Am. Chem. Soc., 122, 2000, 3453, and references therein.;
(b) R. Rao, G.U. Kulkarni, P.J. Thomas, P.P. Edwards, Chem. Eur. J. 8 (2002) 29.
[3] (a) G. Schmid, Chem. Rev. 92 (1992) 1709;
(b) H. Hirai, H. Chawanya, N. Toshima, Reactive Polym. 3 (1985) 127.
[4] V.M. Frolov, Platinum Met. Rev. 40 (1996) 8.
[5] G. Vitulli, P. Pertici, S. Bertozzi, A.M. Caporusso, R. Lazzaroni, P. Salvadori, in: W.A. Herrmann (Ed.), Synthetic Methods of Organometallic and Inorganic Chemistry: Catalysis, Brauer/Herrmann, Munich, 2002, p. 10.
[6] G. Vitulli, E. Pitzalis, R. Lazzaroni, P. Pertici, P. Salvadori, O. Salvetti, S. Coluccia, G. Martra, Mater. Sci. Forum 195 (1995) 93.
[7] S. Pascarelli, F. D'Acapito, G. Antonioli, A. Balerna, F. Boscherini, R. Cimino, G. Dalba, P. Fornasini, G. Licheri, C. Meneghini, F. Rocca, S. Mobilio, ESRF Newslett. 23 (1995) 17.
[8] S. Pascarelli, F. Boscherini, F. D'Acapito, J. Hrdy, C. Meneghini, S. Mobilio, J. Synch. Rad. 3 (1996) 147.
[9] G. Vitulli, G. Uccello-Barretta, P. Pannocchia, A. Raffaelli, J. Organomet. Chem. 302 (1986) C21.
[10] G. Vitulli, E. Pitzalis, P. Pertici, P. Salvadori, S. Coluccia, G. Martra, L. Lampugnani, M. Mascherpa, Mater. Sci. Eng. C 15 (2001) 207.
[11] B. Coq, F. Figueras, Coord. Chem. Rev. 178–180 (1998) 1753.
[12] I. Ojima, M. Tzamarioudaki, C.Y. Tsai, J. Am. Chem. Soc. 116 (1994) 3643.
[13] See as example: P.N. Rylander, Hydrogenation Methods, 1985, 117, Academic Press, New York.
[14] I. Ojima, Chem. Rev. 88 (1988) 1011.
[15] See as example: L. Marchese, G. Martra, S. Coluccia, C.R.A. Catlow, A. Cheetham, New Trends in Materials Chemistry, 1997, p. 79, Kluwer Academic Publishers, London.
[16] C. Louis, L. Marchese, S. Coluccia, A. Zecchina, J. Chem. Soc. Faraday Trans. 185 (1989) 1655.
[17] A. Parmigliana, F. Arena, F. Fruster, S. Coluccia, L. Marchese, G. Martra, A.L. Chuvilin, J. Catal. 141 (1993) 34.
[18] G. Martra, H.M. Swaan, C. Mirodatos, M. Kermarec, C. Louis, Stud. Surf. Sci. Catal. 111 (1997) 617.
[19] D. Martim, D. Duprez, Appl. Catal. A 131 (1995) 297.
[20] H.F.J. van't Blik, J.B.A.D. van Zon, T. Huizinga, J.C. Vis, D.C. Koningsberger, R. Prins, J. Am. Chem. Soc. 107 (1985) 3139.
[21] D.K. Paul, C.D. Marten, Langmuir 15 (1999) 4508.
[22] N. Sheppard, T.T. Nguyen, in: R.J.H. Clark, R.E. Hester (Eds.), Advanced Infrared Spectroscopy of Adsorbed Species, vol. 5, Heyden, London, 1978, p. 67 (Chapter 2).
[23] K.A. Almusaiteer, S.S.C. Chuang, J. Phys. Chem. B 104 (2000) 2265.
[24] P. Basu, D. Panayotov, J.T. Yates, Jr., J. Am. Chem. Soc. 110 (1988) 2074.
[25] E.C. Decanio, D.A. Storm, J. Catal. 132 (1991) 375.
[26] T.S. Zubkov, E.A. Wovchko, J.T. Yates, Jr., J. Phys. Chem. B 103 (1999) 5300.
[27] M. Che, C.O. Bennett, Adv. Catal. 36 (1989) 55.
[28] G. Martra, S. Coluccia, O. Monticelli, G. Vitulli, Catal. Lett. 29 (1994) 105.
[29] A. Balerna, S. Coluccia, G. Deganello, A. Longo, A. Martorana, G. Martra, C. Meneghini, P. Pertici, G. Pipitone, E. Pitzalis, A.M.

Venezia, A. Verrazzani, G. Vitulli, Eur. Phys. J. D 7 (1999) 577.
[30] A. Filipponi, A. Di Cicco, S.R. Natoli, Phys. Rev. B 5 (1995) 15122.
[31] A. Filipponi, A. Di Cicco, Phys. Rev. B 5 (1995) 15135.
[32] (a) M.T. Reetz, W. Helbig, S.A. Quaiser, U. Stimming, N. Breuer, R. Vogel, Science 267 (1995) 367;
(b) T. Yonezawa, T. Tominaga, R. Dominique, J. Chem. Soc. Dalton Trans. (1996) 783.
[33] A. Balerna, A. Longo, A. Martorana, C. Meneghini, S. Mobilio, G. Pipitone, Eur. Phys. J. D 7 (1999) 89.
[34] S. Polizzi, P. Riello, A. Balerna, A. Benedetti, Phys. Chem. Chem. Phys. 3 (2001) 4614.